Reconstruction of source location in a network of gravitational wave interferometric detectors

F. Cavalier, M. Barsuglia, M.-A. Bizouard, V. Brisson, A.-C. Clapson, M. Davier, P. Hello, S. Kreckelbergh, N. Leroy, M. Varvella

HAL Id: in2p3-00099454
https://hal.in2p3.fr/in2p3-00099454v2

Submitted on 28 Sep 2006

Reconstruction of source location in a network of gravitational wave interferometric detectors

Fabien Cavalier,[*] Matteo Barsuglia, Marie-Anne Bizouard, Violette
Brisson, André-Claude Clapson, Michel Davier, Patrice Hello,
Stephane Kreckelbergh, Nicolas Leroy, and Monica Varvella

Laboratoire de l'Accélérateur Linéaire,

IN2P3-CNRS et Université Paris-Sud 11,

Centre Scientifique d'Orsay, B.P. 34, 91898 Orsay Cedex (France)

(Dated: July 14, 2005)

Abstract

This paper deals with the reconstruction of the direction of a gravitational wave source using the detection made by a network of interferometric detectors, mainly the LIGO and Virgo detectors. We suppose that an event has been seen in coincidence using a filter applied on the three detector data streams. Using the arrival time (and its associated error) of the gravitational signal in each detector, the direction of the source in the sky is computed using a χ^2 minimization technique. For reasonably large signals (SNR>4.5 in all detectors), the mean angular error between the real location and the reconstructed one is about $1°$. We also investigate the effect of the network geometry assuming the same angular response for all interferometric detectors. It appears that the reconstruction quality is not uniform over the sky and is degraded when the source approaches the plane defined by the three detectors. Adding at least one other detector to the LIGO-Virgo network reduces the blind regions and in the case of 6 detectors, a precision less than $1°$ on the source direction can be reached for 99% of the sky.

[*]Electronic address: cavalier@lal.in2p3.fr

I. INTRODUCTION

The LIGO and Virgo gravitational wave interferometric detectors are approaching their design sensitivity [1],[2] and in the near future, coincidences between the three detectors (LIGO-Hanford, LIGO-Livingston and Virgo) will be possible. In order to reconstruct the direction of the astrophysical sources in the sky, it is well known [3] that a minimum of three detectors is mandatory even if an ambiguity remains between two positions symmetric with respect to the plane defined by the 3 detectors. The source direction is also provided by the coherent searches for bursts [4], [5], [6] or coalescing binaries [7], [8], [9] where one of the outputs of the detection algorithm is an estimation of the source direction.

In this paper, we propose a method for estimating the source position using only the arrival time of the gravitational signal in each detector. The event detection is supposed to have been previously done by dedicated algorithms ([10-23] for bursts, [24-29] for coalescing binaries) and is not within the scope of this article.

The direction reconstruction is based on a χ^2 minimization as described in Section II. This technique can be easily extended to any set of detectors. Moreover, the method can be applied to several types of sources (burst, coalescence of binary objects ...) as soon as an arrival time can be defined for the event.

Section II also deals with the simulation procedure which will be used in the following sections to evaluate the reconstruction quality in several configurations. Sections III and IV describe the performances of the LIGO-Virgo network first neglecting (III), then including (IV) the angular response of the detectors. In section V, we consider the addition of other gravitational wave detectors (supposing a similar sensitivity) and investigate their impact on the reconstruction. In real conditions, systematic errors on arrival time are likely to exist and their impact on the reconstruction is tackled in Section VI.

II. MODELING THE RECONSTRUCTION OF THE SOURCE DIRECTION

A. Arrival time of GW signals in interferometers

Within a network of n interferometers, we suppose that each detector D_i measures the arrival time t_i of the gravitational wave. Of course, the definition of the arrival time depends on the source type and is a matter of convention, for example: peak value in the case of a

2

supernova signal, end of the coalescence for binary events. In the following, it is assumed that all interferometers use consistent conventions.

The error on the arrival time, σ_i, depends on the estimator used and on the strength of the signal in the detector D_i, strength (for a given distance and a given signal type) which is related to the antenna pattern functions (see [5] and references therein) at time t_i. At that time, the antenna pattern depends on the longitude and the latitude of the detector location, as well as its orientation, the angle between the interferometer arms, the sky coordinates α (Right Ascension) and δ (Declination) of the source, and the wave polarization angle ψ.

The timing uncertainty σ_i can be parametrized by [10]:

$$\sigma_i = \frac{\sigma_0}{(SNR_i)^\varsigma} \tag{1}$$

where SNR_i is the measured SNR in detector D_i, σ_0 and ς are constants depending on the detection algorithm and the signal shape. For example, a burst search with a 1-ms Gaussian correlator leads to $\sigma_0 \simeq 1.4$ ms and $\varsigma = 1$. Typically, for an SNR equal to 10, the error on the arrival time is a few tenth of milliseconds and weakly depends on ς for SNR values between 4 and 10.

B. χ^2 Definition

The n measured arrival times t_i and their associated errors σ_i are the input for the reconstruction of the source direction in the sky, direction defined by α and δ.

In the 3-detector configuration, the angles (θ and ϕ) of the source in the detector coordinate system (see Ref.[4] and [7] for exact definitions) are given by [7]:

$$\begin{aligned}
\sin\theta &= \frac{1}{ab_2}\sqrt{\Delta} \\
\cos\theta &= \pm\frac{1}{ab_2}\sqrt{(ab_2)^2 - \Delta} \\
\sin\phi &= -\frac{b_2(t_1 - t_2)}{\sqrt{\Delta}} \\
\cos\phi &= \frac{a(t_1 - t_3) - b_1(t_1 - t_2)}{\sqrt{\Delta}}
\end{aligned} \tag{2}$$

with

$$\Delta = (b_1(t_1 - t_2) - a(t_1 - t_3))^2 + (b_2(t_1 - t_2))^2 \tag{3}$$

3

where D_1 is placed at $(0,0,0)$, D_2 at $(a,0,0)$ and D_3 at $(b_1,b_2,0)$.

When performing a coherent analysis of the GW detector streams the position of the source in the sky is part of the output parameters, corresponding to the stream combination which maximizes the SNR. However, for a burst search, it is known that thousands of possible positions have to be tested to obtain the solution [5], [6] or a least-square function involving the integration of detector streams has to be minimized [4]. This minimization also implies the test of hundreds of initial conditions in order to reach the right minimum.

Concerning coalescing binaries, it implies the definition of a five-parameter bank of filters including the chirp mass, the three Euler angles and the inclination angle [7] of the orbital plane or a three-parameter bank of thousands filters for the two source angles and the chirp time [9].

In all coherent techniques, the extraction of the source direction is an heavy process imbedded in the detection procedure.

In this paper, we propose a simpler approach where α and δ are found through a least-square minimization using separately triggered events obtained by a coincidence search. We suppose that the detection is already performed applying suitable algorithms (matched filter for coalescing binaries, robust filters for bursts). The χ^2 is defined by:

$$\chi^2 = \sum_{i=1}^{n} \frac{\left(t_i - (t_0 + \Delta_i^{Earth}(\alpha, \delta))\right)^2}{\sigma_i^2} \qquad (4)$$

where t_0 is the arrival time of the gravitational wave at the center of the Earth and $\Delta_i^{Earth}(\alpha, \delta)$ is the delay between the center of the Earth and the ith detector which only depends on α and δ.

The first advantage of this definition is that it deals with absolute times recorded by each detector rather than time differences where one detector has to be singled out. Otherwise, the best choice for the reference detector is not obvious: the detector with the lower error on the arrival time, the detector which gives the larger time delays or the detector leading the best relative errors on timing differences ? This definition leads to uncorrelated errors on fitted measurements.

The second advantage is that the network can be extended to any number of detectors and the addition of other detectors is straightforward. Obviously, the method requires that the event is seen by all detectors.

4

The least-square minimization provides the estimation of t_0, α, δ and the covariance matrix of the fitted parameters. When the number of detectors is greater than 3, the χ^2 value at the minimum can also be used as a discriminating variable, as the system is overconstrained.

C. Simulation procedure for a 3-detector network

A list of coincident events are defined by the three arrival times and their associated errors. No detection procedure is performed in these simulations as stated before.

The simulation proceeds in two steps in order to study two coupled effects: antenna-patterns and location with respect to the 3-detector plane. The first step is a simplified approach: the antenna-pattern functions are ignored and the same error σ_i is assumed for arrival times. The second step is more realistic: we assume the same sensitivity for each detector and the signal strength is adjusted to have the mean (over the three detectors) SNR equal to 10. However, this implies that sometimes, due to the antenna-pattern, the signal is seen in a given detector with an SNR lower than 4.5, which remains an acceptable threshold for a real detection. The same threshold equal to 4.5 will be used later to see the effect of a reasonable detection scheme on the angular reconstruction error. We evaluate the errors σ_i for each arrival time t_i using Equation 1 with $\zeta = 1$.

For a given simulation, the coordinates $(\alpha^{true}, \delta^{true})$ of the source are chosen and the true arrival times t_i^{true} on each detector are computed taken t_0^{true} equal to 0 (it is obvious that the timing origin can always been chosen such as $t_0^{true} = 0$)

The measured arrival times $t_i^{measured}$ are drawn according to a Gaussian distribution centered on t_i^{true} and of width σ_i. The simulated values $t_i^{measured}$ are then used as inputs for the least-square minimization. As the minimization is an iterative procedure, some initial values for the parameters have to be given. t_0 is initialized by the average of $t_i^{measured}$. For the angles, it appears that the initial values for the angles have no influence on the minimization convergence and a random direction is adequate. In the case of three interferometers, it is well known that there is a twofold ambiguity for the direction in the sky which can lead to the same arrival times in the detectors. These two solutions are symmetric with respect to the 3-detector plane. In order to resolve the ambiguity, a fourth detector is needed. For the evaluation of the reconstruction accuracy, only the solution closest to the source is retained.
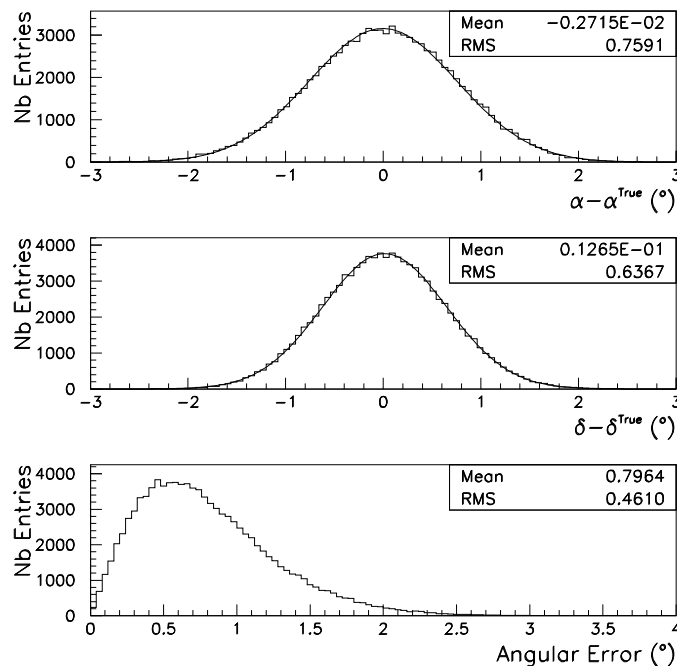
FIG. 1: Reconstruction accuracy for a source at the Galactic Center at a fixed day time for LIGO-Virgo network.

The angular error is the angular distance on the sphere between the true direction and the reconstructed one. The curves on the first two plots correspond to the best Gaussian fit.

III. SOURCE DIRECTION RECONSTRUCTION: 3-DETECTOR NETWORK GEOMETRY

In this section, we only deal with the LIGO-Virgo network and the effect of the antenna-pattern functions are not included and it is assumed that all detectors measure the arrival time with the same precision. As previously said, it allows to decouple the effect of the antenna-patterns and of the location with respect to the 3-detector plane.

First of all, as an example, in order to evaluate the accuracy of the reconstruction, we choose a given position in the sky (coordinates of the Galactic Center $\alpha_{GC} = 266.4°, \delta_{GC} = -28.98°$) and we perform the simulation with $\sigma_i = 10^{-4}$ s at a fixed time. The results are shown on Figure 1. A resolution of about 0.7 degrees can be achieved both on α and δ. The angular error is defined as the angular distance on the sphere between the true direction and the reconstructed one (it does not depend on the coordinate system and in particular there

6

is no divergence (only due to the coordinate system) when δ is equal to 90 degrees). This variable will be used in the following steps as the estimator of the reconstruction quality. The mean angular error is 0.8 degrees. As shown on Table I, the estimated errors (given by the covariance matrix) obtained by the χ^2 minimization are in perfect agreement with these resolutions.

Angle	RMS of Distribution	Mean of estimated errors given by the covariance matrix
α	0.760°	0.758°
δ	0.635°	0.636°

TABLE I: Reconstruction accuracies on α and δ and errors given by the covariance matrix. Three digits are given in order to show the adequacy between RMS and errors given by the covariance matrix.

Varying σ_i in the simulation, it is found that the resolution is proportional to the timing resolution for reasonable errors ($\sigma_i \leq 3$ ms. For $\sigma_i \gg 3$ ms, the errors become comparable to the sky size.) and we obtain:

$$\alpha_{Resolution} = 0.7° \ \frac{\sigma_i}{10^{-4}\text{s}}$$
$$\delta_{Resolution} = 0.6° \ \frac{\sigma_i}{10^{-4}\text{s}} \tag{5}$$
$$\text{Mean Angular error} = 0.8° \ \frac{\sigma_i}{10^{-4}\text{s}}$$

For the Galactic Center direction and with $\sigma_i = 0.1$ ms, we evaluate the reconstruction performances over one entire day, still neglecting the antenna-pattern.

It clearly appears on Figure 2 that the resolution varies, as expected, during the day and lies between 0.8° and 4.3° (see Table II for details).

The error maximum which appears around $t = 20$h (the time origin is arbitrary) corresponds to directions for which the source approaches the detector plane. The angular distance between the two possible solutions (the source and its mirror image) gives a good estimator of this closeness (see Fig. 2). This effect is even clearer on Figure 3 where the source is located at $\delta = 0°$. In this case, the source crosses the 3-detector plane twice a day ($t = 2.4$ h, $t = 14.4$ h) and the angular distance between the real source and its mirror image
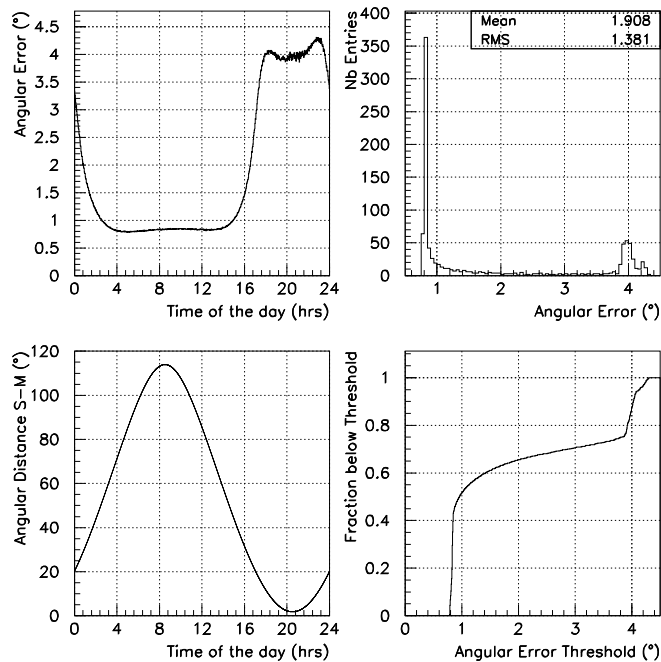
7

FIG. 2: Angular Error for a source at the Galactic Center for one day (t=0 arbitrary chosen) for LIGO-Virgo network.

The top-left plot presents the angular error as a function of time. The bottom-left plot shows the angular distance between the source (S) and its mirror image (M) (other direction in the sky which gives the same time delays). The top-right plot is the distribution of angular errors. The bottom-right gives the fraction of events with an angular error below a given threshold versus this threshold. σ_i is set to 0.1 ms for all detectors.

is null. This degradation of the angular reconstruction is not related to the χ^2 minimization technique. It is a geometrical property of the network which releases constraints when the source belongs to the 3-detector plane. For the $\delta = 0°$ configuration, angular resolutions as given in Table II are similar to the ones obtained for the Galactic Center.

This degradation can be easily understood with only two detectors located at $(\pm d/2, 0, 0)$ and a source in the (x,y) plane defined by its angle θ with the x axis. In this 2-detector case, the arrival time difference t_{21} is given by:

$$t_{21} = \frac{d}{c} \cos \theta \tag{6}$$

and thus, if t_{21} is measured with an error δt, it will induce an error $\delta\theta = \frac{c\delta t}{d|\sin\theta|}$ on the

8

$\delta(°)$	Minimal Error (°)	Maximal Error (°)	Mean Error (°)	Median Error (°)
-28.98 (GC)	0.8	4.3	1.9	0.95
0	1.3	3.1	1.8	1.5
All values	0.7	4.5	1.6	1.1

TABLE II: Angular resolution for Galactic Center, $\delta = 0°$ position and averaged on all possible values of δ taken over the whole day. No antenna-pattern effect is included.

source direction which diverges when the source belongs to the 2-detector line ($\theta = 0$ or π). Of course, this simple estimation of the angular error supposes that Eq. 6 between t_{21} and θ can always be inverted, assumption which fails when t_{21} becomes greater than $\frac{d}{c}$ due to measurement errors. We can wonder how to handle this case. In the 2-detector example, we minimize χ^2 defined by:

$$\chi^2(\theta) = \frac{1}{\delta t^2} \left(t_{21}^{measured} - \frac{d}{c} \cos \theta \right)^2 \qquad (7)$$

which becomes minimal for $\theta = \mathrm{acos}(t_{21}^{measured} \times \frac{c}{d})$ if $|t_{21}^{measured} \times \frac{c}{d}| \leq 1$ or $\theta = 0$ when the previous condition is not satisfied. We observe similar effect in the 3-detector case when the source approaches the 3-detector plane.

Figure 4 presents the angular errors averaged on all possible value of δ. In this case, the angular resolutions are given in Table II, ranging 0.7 to 4.5 degrees. Without considering antenna-pattern effect, it means that an angular error lower than about one degree can be reached for half of the sky and 90 % is below 3.5 degrees. The intersection of the 3-detector with the celestial sphere appears as a zone with worst angular resolutions (error ranging from 3 degrees to 4.5 degrees) of the source direction.

IV. INCLUDING THE ANTENNA-PATTERN EFFECT IN A 3-DETECTOR NETWORK

As in previous section, we use the LIGO-Virgo network as benchmark. Now, the strength of the signal seen by each detector is computed taking into account the antenna-pattern functions. The errors on arrival times are estimated using Eq.1 with $\zeta = 1$ and $\sigma_0 = 1\mathrm{ms}$. In order to remain close to the case described in Section III (all timing errors equal to
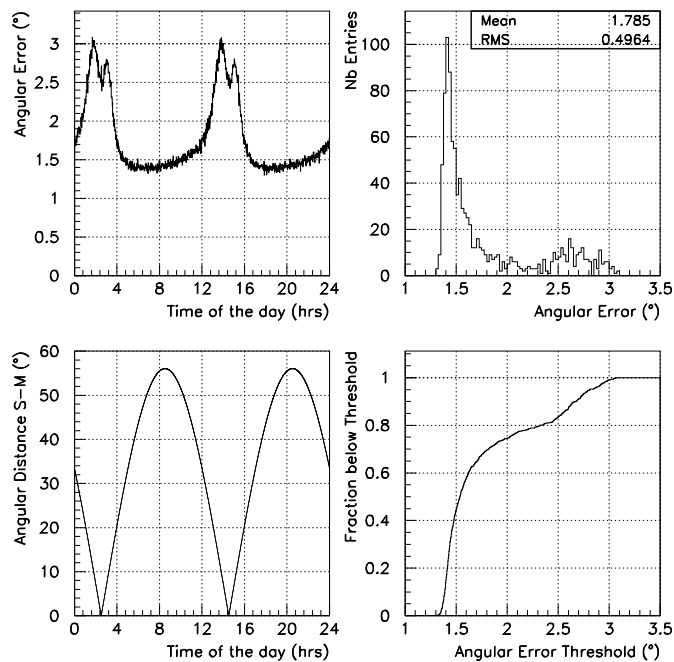
FIG. 3: Angular error for a source at $\delta = 0°$ for one day (t=0 arbitrary chosen) for LIGO-Virgo network.

The top-left plot presents the angular error as a function of time. The bottom-left plot shows the angular distance between the source (S) and its mirror image (M) (other direction in the sky which gives the same time delays). The top-right plot is the distribution of angular errors. The bottom-right gives the fraction of events with an angular error below a given threshold versus this threshold. σ_i is set to 0.1 ms for all detectors.

0.1 ms), we impose that the mean SNR over the three detectors is equal to 10. A linear polarization has been assumed for the incoming signal.

Figure 5 presents the angular error as a function of the day time for a source located at $\delta = 0°$ and can be compared to Fig. 3. The two broad peaks ($t = 2.4$ hours and $t = 14.4$ hours), corresponding to the time when the source belongs to the 3-detector plane, are still present (barely seen due to the change of scale) but six sharp diverging peaks show up. They correspond to blind regions for at least one detector, as expected.

Of course, in real conditions, a minimal threshold will be applied for the event selection. For this purpose, we define a SNR threshold equal to 4.5 on each detector which leads
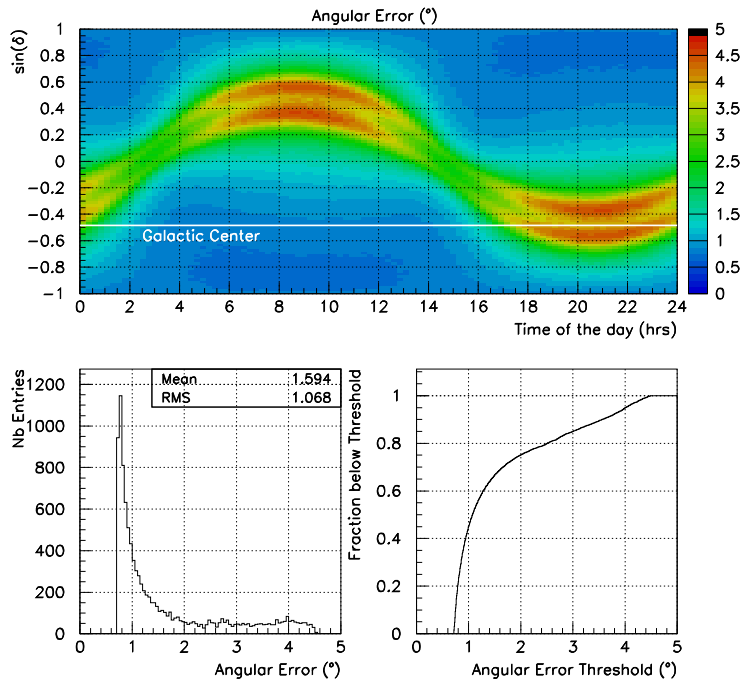
FIG. 4: Reconstruction resolution for the whole sky for LIGO-Virgo network.
The top plot presents the angular error as a function of time for all possible values of δ. The bottom-left plot is the distribution of angular errors. The bottom-right gives the fraction of events with an angular error below a given threshold versus this threshold. The white line gives the trajectory of the Galactic Center during the day. σ_i is set to 0.1 ms for all detectors.

(supposing a Gaussian noise) to a false alarm rate about 10^{-6} Hz when requiring a triple coincidence between Virgo, LIGO-Hanford and LIGO-Livingston. About 79 % of the events satisfy this constraint and a median error of 2.0° is reached (See Table III and Fig. 6).

For a source located at the Galactic Center, the angular error shows several spikes related to the antenna-pattern effect and the geometry of the network only increases the mean error in the region around $t = 21$ h (Fig. 7). All peaks correspond to regions which are blind for at least one interferometer. Imposing that all SNR are above 4.5 leaves 56.4 % of the events and in particular all these blind regions are removed. The obtained angular resolutions are given in Table III. They are slightly better than for the $\delta = 0°$ case.

Figure 8 presents the angular errors averaged on all possible δ. As in Fig. 4, the intersection between the 3-detector plane and the celestial sphere is visible. The regions of
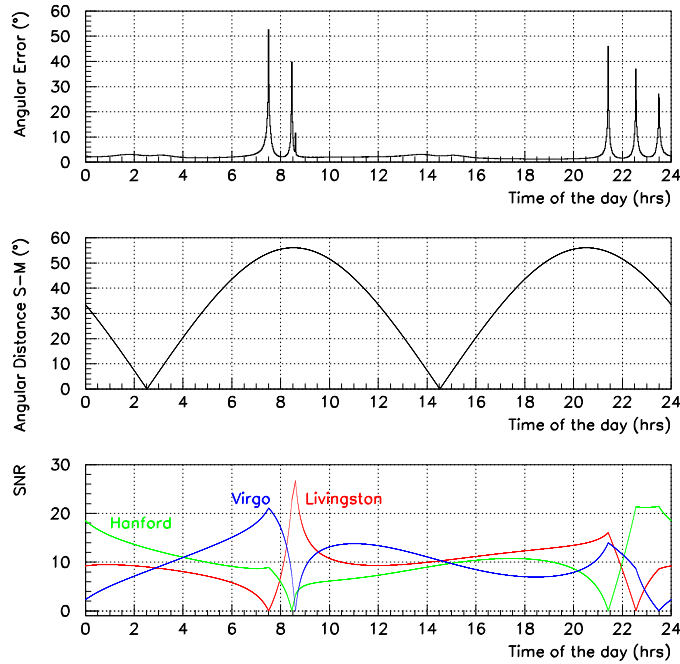
FIG. 5: Angular Error for a source at $\delta = 0°$ as a function of the day time (t=0 arbitrary chosen) for LIGO-Virgo network.

The top plot presents the angular error as a function of time. The middle plot shows the angular distance between the source and its mirror image (the other sky direction giving the same time delays). The SNR values in each interferometer are plotted on the bottom figure. The effect of the antenna-pattern functions is included and the mean SNR is set to 10.

largest errors ($> 15°$) corresponds to the blind regions of the various detectors. Without any conditions on the SNR in each detector, we obtain a median error of 1.7° (see Table III). The SNR condition is satisfied for 60% of the events and leads to a median error of 1.3° with 90 % of the events below 3.7°. In the most favorable cases, we can even reach a precision of 0.7°. A resolution better than 1° is obtained in 30% of the cases.

V.   ADDITION OF OTHER GRAVITATIONAL WAVE DETECTORS

First of all, the 2-kilometer long Hanford interferometer has been included in the network. In this case, we supposed that the SNR seen by by Hanford 2k is half of the SNR seen by Hanford 4k. As expected, adding Hanford 2k does not change significantly the resolutions
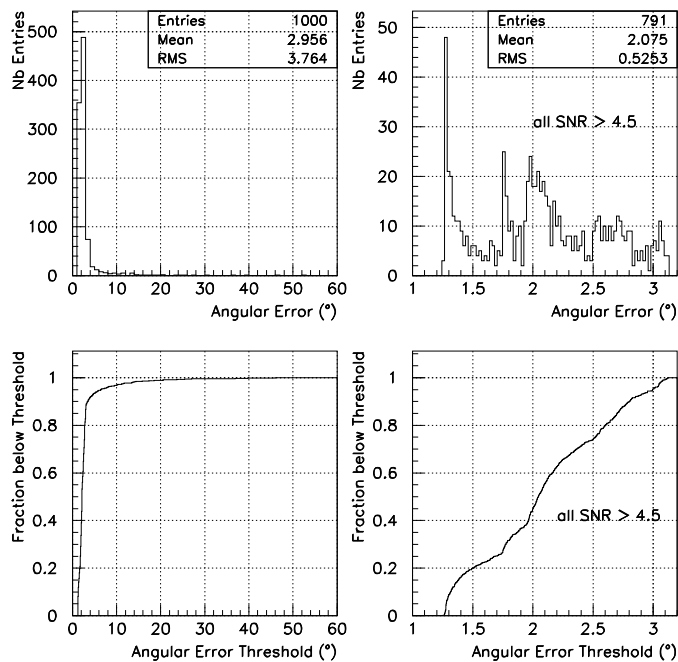
12

FIG. 6: Distribution of angular errors for a source at $\delta = 0°$ for LIGO-Virgo network.
The top-left plot shows the distribution of angular error for all events. The bottom-left one presents
the fraction of events with an angular error below a given threshold versus this threshold. The
right plots are the same imposing that the SNR seen by each detector is greater than 4.5.

obtained in previous sections.

Then, we add TAMA [30], GEO [31] and AIGO [32] assuming (for sake of simplicity) the
same sensitivities as LIGO and Virgo. We still impose a mean SNR equal to 10. Figure 9,
which has to be compared to Figure 5, shows the angular reconstruction for a source located
at $\delta = 0°$ as a function of the day time adding only a fourth detector to the LIGO-Virgo
network. Of course, there is no longer an ambiguity in the possible solutions and all former
blind regions are attenuated except the one around $t = 8.5h$ for which effective low SNRs
are obtained with both Hanford and Virgo. The mean error (3° for LIGO-Virgo Table III) is
lowered to 2.0° adding GEO, to 1.7° adding TAMA and 0.7° adding AIGO. Not surprisingly,
the larger the network baseline, the better the resolution.

In order to evaluate the performances of a strongly overconstrained network, we evaluate
the reconstruction resolution for the full sky using the 6 detectors (still using the same

13

$\delta(°)$	Event Fraction(%)	Min. Error (°)	Mean Error (°)	Median Error (°)
-28.98 (GC) Any SNR	100	0.7	4.0	1.8
-28.98 (GC) All SNR $\geq$ 4.5	56.4	0.7	1.8	1.25
0 Any SNR	100	1.2	3.	2.2
0 All SNR $\geq$ 4.5	79.1	1.2	2.1	2.
All values Any SNR	100	0.7	2.7	1.7
All values All SNR $\geq$ 4.5	59.8	0.7	1.8	1.3

TABLE III: Angular resolution for Galactic Center, $\delta = 0°$ position and averaged on all possible values of δ taken over the whole day. The antenna-pattern effect is included. The column "Event Fraction" gives the fraction of events satisfying the SNR selection criterion.

sensitivity). The results are shown in Figure 10 similar to Figure 8. The mean error is about 0.4° and 99% of the sky is covered with a resolution below 0.8°. The regions with errors between 1 and 3 degrees correspond to directions for which several interferometers have very low SNRs (as the region around $t = 8.5h$ in the previous figure).

VI.   EFFECTS OF SYSTEMATIC ERRORS ON ARRIVAL TIMES

All angular errors quoted previously suppose that arrival time measurements are only subject to Gaussian noise. Systematic biases can also be introduced by the analysis and their effect can be evaluated. In order to do so, we modify Equation 8 introducing a timing bias for only one detector:

$$t_i^{Measured} = t_i^{true} + GaussianRandom \times \sigma_i + Bias \qquad (8)$$

As in sections III and IV, we only consider the LIGO-Virgo network. It appears that
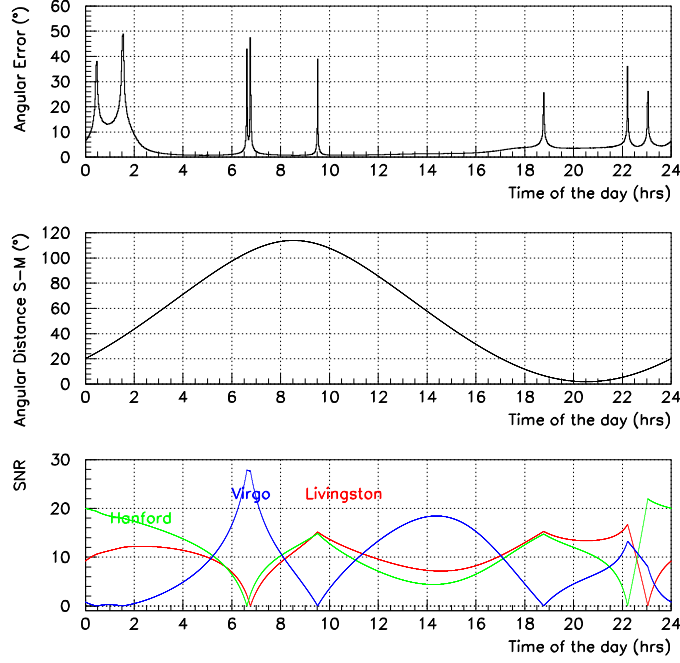
FIG. 7: Angular Error for a source at the Galactic Center as a function of the day time (t=0 arbitrary chosen) for LIGO-Virgo network.

The top plot presents the angular error as a function of time. The middle plot shows the angular distance between the source and its mirror image (the other sky direction giving the same time delays). The values of the antenna-pattern functions are plotted on the bottom figure. The effect of the antenna-pattern functions is included and the mean SNR is set to 10.

Bias (ms)	Bias on $\alpha(°)$	Bias on $\delta(°)$	Angular Bias (°)
.1	-0.24	0.65	0.68
.2	-0.48	1.26	1.33
.3	-0.72	1.79	1.90
.4	-0.97	2.55	2.69
.5	-1.2	3.17	3.35
1.	-2.6	6.20	6.63

TABLE IV: Effect of a timing bias on angular reconstruction.

The bias is applied to the arrival time at Livingstone interferometer. The RMS of the statistical errors has been set to .1 ms. For this direction, the statistical angular error is about 0.8°.
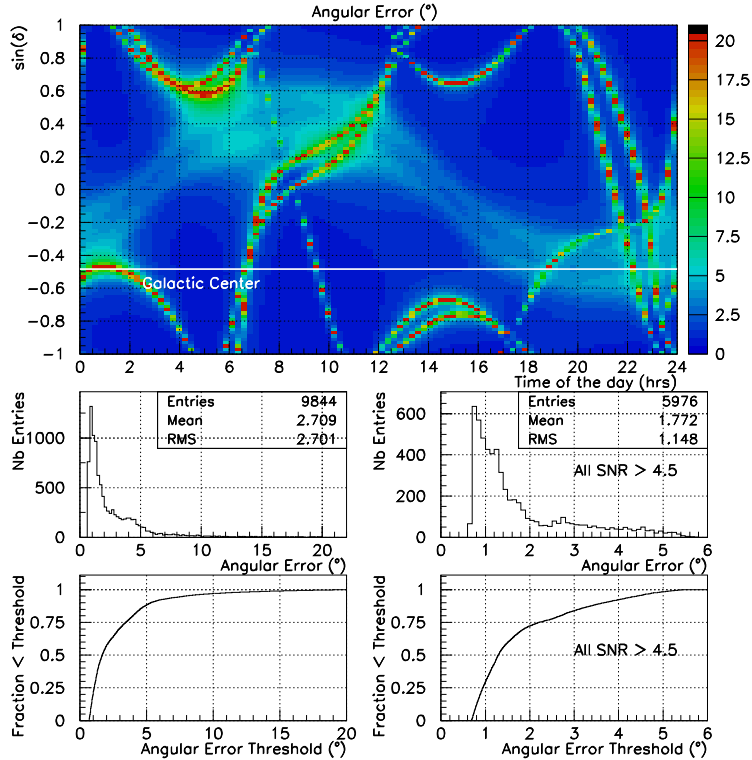
15

FIG. 8: Reconstruction resolution for the full sky for LIGO-Virgo network. The top graph gives the angular error as a function of α and $\sin(\delta)$. For clarity, the values above $20°$ have been set to $20°$. The bottom plots presents the angular error distribution and the fraction of events below a given angular threshold imposing or not the SNR condition (all SNR>4.5).

the widths of the distribution for reconstructed α and δ are not modified by the bias but the central values are shifted from the true ones. The differences between the reconstructed value and the true one are proportional to the bias and are significantly different from zero when the bias and the statistical error have the same order of magnitude. Table IV shows the effect of the bias for a given direction (we check that the effect is independant of the source location). In this example, the bias has been applied to the Livingstone interferometer. The width of statistical errors on arrival time was .1 ms leading to a statistical angular error about $0.8°$. For the tested configurations, we do not observe significant differences between the three interferometers of the network.
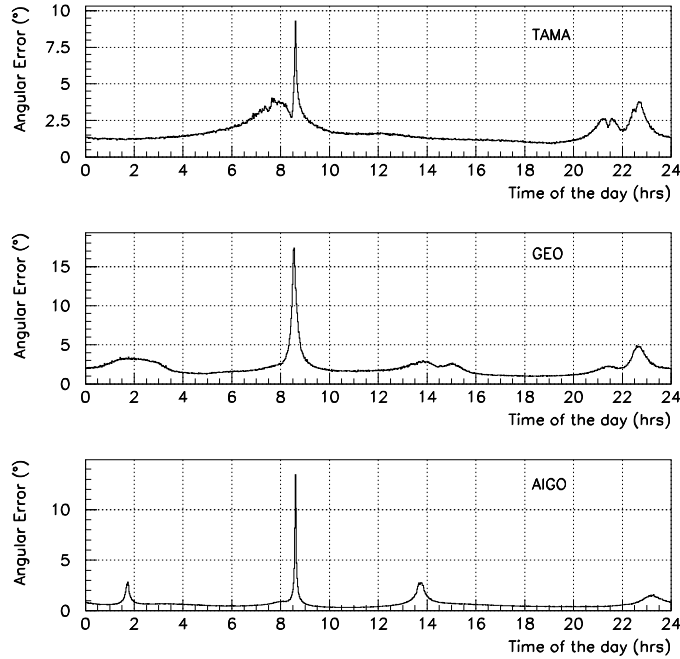
FIG. 9: Reconstruction resolution for a source at $\delta = 0°$ as a function of the day time (t=0 arbitrary chosen) adding a fourth detector to the LIGO-Virgo network.

The top figure presents the angular error as a function of time adding TAMA, the middle one adding GEO and the bottom one adding AIGO.

VII. CONCLUSION

We described a method for the reconstruction of the source direction using the timing information (arrival time and associated error) delivered by gravitational wave detectors such as LIGO and Virgo. The reconstruction is performed using a least-square minimization which allows to retrieve the angular position of the source and the arrival time at the center of the Earth. The minimization also gives an estimation of errors and correlations on fitted variables. For a given position, the angular error is proportional to the timing resolution and the systematic errors (if they exist) introduce a significant bias on reconstructed angles when they reach the level of the statistical one.

When the antenna-pattern effect is included and imposing a mean SNR value of 10 in the LIGO-Virgo network, a precision of 1.7° can be reached for half of the sky. In order to reproduce a realistic case, we apply a threshold on the SNR in each detector (SNR> 4.5
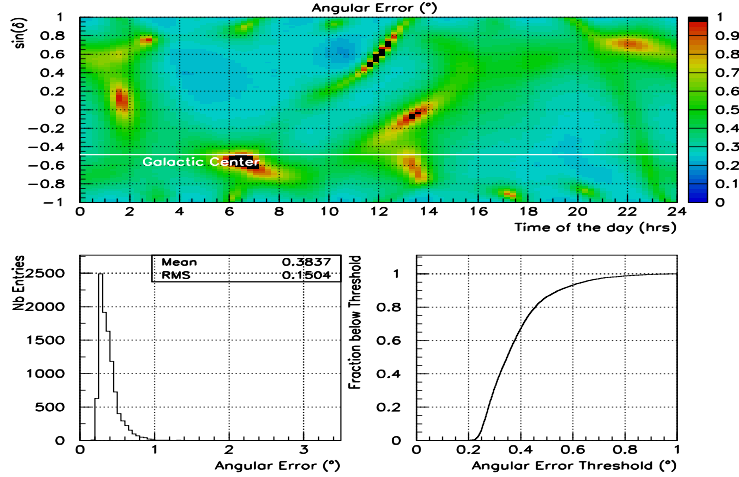
17

FIG. 10: Reconstruction resolution for the full sky with a network of 6 detectors. The top graph gives the angular error as a function of α and $\sin(\delta)$. For clarity, the values above $1°$ have been set to $1°$. The bottom plots presents the angular error distribution and the fraction of events below a given angular threshold.

leading to a false alarm rate about 10^{-6} Hz when performing a threefold coincidence). This condition is satisfied for 60 % of the sky and the median angular error in this case is $1.3°$. As a resolution of $1°$ is obtained for 30 % of the events satisfying the SNR condition, it means that about 20 % of the whole sky is seen with an angular error lower than $1°$.

Adding other gravitational waves detectors allows to reduce the blind regions and to lower the mean resolution. In the best considered case (6 detectors), the resolution is about $0.4°$ and 99% of the sky is seen with a resolution lower than $0.8°$.

All quoted resolutions (about one degree) are similar to those delivered by γ-ray satellites when the first GRB counterparts have been identified. So, we can expect it will be also sufficient for the first identification of gravitational wave sources.

[1] B.Abbot et al, NIMA **517**, (2004). http://www.ligo.caltech.edu

[2] F.Acernese et al, Class. Quantum Grav. **22**, S869 (2005). http://wwwcascina.virgo.infn.it

[3] J.L. Boulanger et al, A&A **217**, 381 (1989).

[4] Y. Gürsel and M. Tinto, Phys. Rev. **D40**, 3884 (1989).

[5] N. Arnaud et al, Phys. Rev. **D68**, 102001 (2003).

[6] J. Sylvestre, Phys. Rev. **D68**, 102005 (2003).

[7] P. Jaranowski and A. Krolak, Phys. Rev. **D49**, 1723 (1994).

[8] R. Balasubramanian, B.S. Sathyaprakash and S. V. Dhurandhar, Pramana J. Phys., L436 (1995).

[9] A. Pai, S. Dhurandhar, and S. Bose, Phys. Rev. **D64**, 042004 (2002).

[10] N. Arnaud et al, Phys. Rev. **D67**, 062004 (2003).

[11] E.E. Flanagan and S.A Hughes, Phys. Rev. **D 57**, 4535 (1998).

[12] W.G. Anderson and R. Balasubramanian Phys. Rev. **D 60**, 102001 (1999).

[13] W.G. Anderson, P.R. Brady, J.D.E. Creighton, and E.E. Flanagan, Int. J. Mod. Phys. **D 9**, 303 (2000).

[14] S.D. Mohanty, Phys. Rev. **D 61**, 122002 (2000).

[15] W.G. Anderson, P.R. Brady, J.D.E. Creighton, and E.E. Flanagan, Phys. Rev. **D 63**, 042003 (2001).

[16] A. Vicere, Phys. Rev. **D 66**, 062002 (2002).

[17] J. Sylvestre, Phys. Rev. **D 66**, 102004 (2002).

[18] M.Ando et al, Class.Quantum Grav. **21**, S1679 (2004).

[19] S.Klimenko and G.Mitselmakher, Class.Quantum Grav. **21**, S1685 (2004).

[20] J.W.C McNabb et al, Class.Quantum Grav. **21**, S1705 (2004).

[21] S.Chatterji et al, Class.Quantum Grav. **21**, S1809 (2004).

[22] S.Klimenko and G.Mitselmakher, Class.Quantum Grav. **21**, S1819 (2004).

[23] P.R.Brady and S.Ray-Majumder, Class.Quantum Grav. **21**, S1839 (2004).

[24] C.Cutler and E.E.Flanagan, Phys. Rev. **D 49**, 2658 (1994).

[25] E.Poisson and C.M.Will, Phys. Rev. **D 52**, 848 (1995).

[26] B.J.Owen, Phys. Rev. **D 53**, 6749 (1996).

[27] S.D.Mohanty, Phys. Rev. **D 57**, 630 (1998).

[28] B.J.Owen and B.S.Sathyaprakash, Phys. Rev. **D 60**, 022002 (1999).

[29] F.Marion, Proceeding of the Rencontres de Moriond 2003 (2004).

[30] TAMA Collaboration, Class. Quantum Grav. **21**, S403 (2004). http://tamago.mtk.nao.ac.jp/tama.html

[31] GEO Collaboration, Class. Quantum Grav. **23**, S71 (2006). http://www.geo600.uni-

hannover.de

[32] ACIGA Collaboration, Class. Quantum Grav. **23**, S41 (2006). http://www.anu.edu.au/Physics/ACIGA